RESEARCH MEMORANDUM

A FREE-FLIGHT INVESTIGATION OF THE EFFECTS OF SIMULATED

SONIC TURBOJET EXHAUST ON THE DRAG OF A BOATTAIL BODY

WITH VARIOUS JET SIZES FROM MACH NUMBER 0.87 TO 1.50

By Ralph A. Falanga

Langley Aeronautical Laboratory
Langley Field, Va.

NATIONAL ADVISORY COMMITTEE
FOR AERONAUTICS
WASHINGTON

NATIONAL ADVISORY COMMITTEE FOR AERONAUTICS

RESEARCH MEMORANDUM

A FREE-FLIGHT INVESTIGATION OF THE EFFECTS OF SIMULATED

SONIC TURBOJET EXHAUST ON THE DRAG OF A BOATTAIL BODY

WITH VARIOUS JET SIZES FROM MACH NUMBER 0.87 TO 1.50

By Ralph A. Falanga

SUMMARY

Three $7.5°$ boattail bodies of revolution with varying base-annulus areas and jet sizes provided with simulated-turbojet-exhaust rocket motors were flight-tested to determine the jet interference effects on drag over a Mach number range from approximately 0.87 to 1.5. The results indicated that in the transonic and low-supersonic speed range the jet caused positive pressure increments on the base and boattail which appreciably reduced the configuration drag from the power-off condition. At the higher supersonic speeds, the jet caused positive pressure increments only on the base and resulted in a smaller reduction in body drag from power-off conditions.

In the present tests the jet size appears to play a secondary role in reducing drag for an average jet static-pressure ratio of 3.65.

INTRODUCTION

Modern high-speed airplanes have penetrated the supersonic flight regime, and an increasing amount of interest is being directed toward the effects propulsive jets have on the external drag of housings for turbojet engines, since this can represent an appreciable percentage of the total drag. Data on base pressures and boattail drag have been reported in references 1 to 7 where it has been shown that the afterbody drag can be appreciably higher than the forebody drag of the configurations and that large drag savings may be realized, depending on the afterbody configuration, nozzle design, and jet operating conditions.

At present, there is no completely adequate analytical method available other than the semiempirical theories for calculating or predicting base pressures caused by the jet. Most of the systematic

investigations reported thus far (refs. 1 to 7) have been made at
supersonic velocities and little information is available in the
transonic and low-supersonic speed range (ref. 8) in which present-
day jet aircraft are operating.

The present investigation was conducted by the Langley Pilotless
Aircraft Research Division to determine the effects of a jet issuing
from a rocket, designed to simulate turbojet exit conditions, on body
drag through the transonic and low-supersonic speed range.

Three research models with the same external configuration but
with varying jet sonic-exit sizes propelled with turbojet simulators
(designed according to ref. 9) were free-flight-tested at zero angle
of attack at the Langley Pilotless Aircraft Research Station, Wallops
Island, Va.

The Mach number range covered from 0.875 to 1.5, and the Reynolds
number range covered from 25×10^6 to 53.5×10^6, based on body length.

SYMBOLS

A   area, sq ft

S   maximum cross-sectional area, sq ft

a   acceleration, ft/sec^2

g   acceleration due to gravity, ft/sec^2

γ ratio of specific heats

M   Mach number

p   static pressure, lb/sq ft abs

R   Reynolds number based on body length

C_p pressure coefficient, $\dfrac{p - p_0}{q}$

C_D drag coefficient, $D/q_0 S$

q_0 dynamic pressure, $\dfrac{\gamma p M^2}{2}$, lb/sq ft

T   thrust, lb

D   drag, lb

W   weight, lb

θ   flight-path angle, deg

Subscripts:

o   free stream

j   jet exit

b   base

t   rocket throat

a   base annulus

T   total

i   instantaneous

L   longitudinal

DESCRIPTION OF MODELS

Models 1, 2, and 3 had a ratio of jet to base area of 0.844, 0.706, and 0.563, respectively. Details and dimensions of the configurations are given in figure 1. The fuselage was identical for all three models and consisted of a parabolic nose joined to a 6.50-inch-diameter cylindrical body with a conical boattail. The parabolic nose section, coordinates of which are given in table I, was 26.00 inches long, and the straight cylindrical section was 28.03 inches in length. The conical afterbody had a 7.5° boattail angle and was 10.97 inches long. Four thin 60° sweptback fins with beveled leading and trailing edges attached to the conical afterbody were used to stabilize the body in flight. The body total length was 65.00 inches for all three models. Photographs of the external configuration are shown in figure 2.

A comparison of the differences in base annuli for the models tested is revealed in figure 3. Also shown in this figure is a view of the base static-pressure tube used to measure base pressure.

Figure 4 shows a cross section of a typical turbojet simulator used in flight. It consisted essentially of a combustion chamber, a flow-control nozzle, a plenum chamber, and a convergent sonic-exit section. The simulator utilized a modified 3.25-inch aircraft rocket combustion chamber containing a specially machined cordite SU/K propellant. The throat and exit diameters are also listed in figure 4. The base and motor static-pressure tubes used for flight measurements were located as shown in figure 4.

TESTS AND INSTRUMENTATION

The models were launched from a rail-type launcher at approximately a 60° angle as shown in figure 2(b). A single 65-inch HVAR rocket motor boosted the models to supersonic speeds. After separation from the booster, the models decelerated to a Mach number of approximately 0.85 before the turbojet simulator was fired which accelerated the models to their peak Mach numbers.

A four-channel telemeter which was carried in the nose of each model continuously transmitted measurements of base static pressure, motor static pressure, and low- and high-range longitudinal-accelerometer data to the ground receiving stations. Flight data were also obtained from CW Doppler velocimeter, SCR 584 radar, tracking cameras, and radiosonde. These data were used to obtain total drag coefficients, Mach number, and free-stream static pressure (by methods described in ref. 10) as well as base pressure and base drag coefficients.

Static firings were performed on each of the turbojet simulators used in the flight models to determine whether each unit met the specified engine parameters. Reference 9 gives the method used in simulating required engine exit parameters. The turbojet exhaust parameters simulated by these units were jet thrust, weight flow, and jet static-pressure ratio. The exhaust-gas stagnation temperature for these units was approximately 4,000° R, and the specific-heat ratio was approximately 1.25. These scaled-down parameters simulated approximately those of a current full-scale turbojet engine with afterburner operating at an altitude of 35,000 feet and a free-stream Mach number of 1.2.

ANALYSIS

The thrusts of the rocket motors during flight tests were computed by using the following equation:

$$T_j = p_j A_j (\gamma M_j{}^2 + 1) - p_o A_j \qquad \qquad (1)$$

The rocket motor for each flight model was statically test-fired at the Langley rocket test cell. A calibration curve of jet exit static pressure p_j was established from these tests as a function of a motor static pressure whose orifice location is as shown in figure 4. These calibration curves were then used along with measurements of motor static and free-stream static pressure to obtain the thrust during flight.

The power-on drag coefficients were determined from the following equation:

$$C_D = \frac{T_j - W_i\left(\dfrac{a_L}{g} + \sin\theta\right)}{qS} \qquad \qquad (2)$$

where the net acceleration and flight-path angle were obtained directly from flight measurements and the thrust was computed from equation (1).

The base pressure coefficients referenced to free-stream conditions were obtained from the following relationship:

$$C_{p_b} = \frac{p_b - p_o}{q_o} \qquad \qquad (3)$$

The base drag coefficients for power-off and power-on conditions referenced to maximum body area were computed according to the following equations:

For power off

$$C_{D_b} = -C_{p_b}\frac{A_b}{S} \qquad \qquad (4a)$$

For power on

$$C_{D_b} = -C_{p_b}\frac{A_a}{S} \qquad \qquad (4b)$$

TEST ACCURACY

To establish telemeter instrument accuracies over a number of years, statistical data have been compiled on instrument measurements,

and on this basis it is believed that the maximum probable error of
each measurement is within ±1 percent of full-scale range.

The basic accuracy of the power-off drag coefficients presented
herein has been established by comparison of the individual drag-
coefficient curves of the three similar models. Any deviation in drag
coefficients which existed for these curves could have been caused by
model dissimilarities in construction and finish, and/or instrumentation
errors of the CW Doppler velocimeter, tracking radar, telemeter, and
radiosonde. A power-off drag-coefficient curve was established by
using the root-mean-square values of drag coefficients of the individual
models. The maximum probable errors for the individual-model drag coef-
ficients were then taken as the maximum deviation of any one of the
three curves from the root-mean-square drag-coefficient curve. On the
basis of the foregoing, the test accuracies are within the values tabu-
lated as follows for the power-off condition:

M	ΔM	Fuselage C_{p_b}	Measured C_D
0.95	±0.010	±0.0100	±0.0095
1.25	±.005	±.00526	±.0025
1.40	±.005	±.00413	±.0025

The degree of accuracy obtained for computed power-on drag coef-
ficients was based mainly on the accuracy with which the thrusts of
the rocket motors were computed, since the absolute values of the thrust
were four to six times greater than those of the drag for all models
tested. It was conceivable that a maximum probable error of ±10 pounds
of thrust could have been inherent in the technique used for obtaining
absolute values of flight thrust. This corresponds to an error in power-
on drag coefficients of ±0.04 at $M = 0.95$ and ±0.02 at $M = 1.3$ for
all models tested.

RESULTS AND DISCUSSION

The Mach number range covered by these flight models varied from
approximately 0.875 to 1.5. The Reynolds number based on body length
varied from 27×10^6 to 53.5×10^6 during the power-off period and for
the power-on period from 25×10^6 to 40.75×10^6 as shown in figure 5.
The range of Reynolds number covered by all models indicates that the
boundary layer near the base was turbulent.

The variations of total drag coefficient, base drag coefficient, and base pressure coefficient (for power off and power on) and jet static-pressure ratio with free-stream Mach number are presented in figures 6, 7, and 8 for models 1, 2, and 3, respectively. The total power-off drag coefficients for these three similar models are in agreement with each other.

Jet interference effects on body drag of the configurations have resulted in considerably lower power-on drag coefficients throughout the Mach number range of these tests. At transonic or low supersonic speeds the reduction in drag is much greater than at the higher supersonic speeds. The difference in drag at the higher supersonic speeds between the power-off and power-on phases is approximately equal to the magnitude of the difference in base drag as can be seen in the plots of base drag coefficients in figures 6, 7, and 8. Coefficients of base pressure for the power-on phases remain positive (in the direction of thrust) throughout the test Mach number range, whereas the power-off base pressure coefficients are positive below $M = 1$ and then become negative throughout the rest of the test range.

Differences in drag at transonic or low supersonic speeds between power-off and power-on conditions are greater than the change in base drag alone. These differences range between three to five times greater than the difference in base drag. It is felt that positive pressure increments acted on part of the boattail to cause these noted reductions in drag in this speed range. Reference 8 reported the same general trends in this speed range, except that the magnitude of the difference was not so pronounced. This could have been due to the fact that the jet static-pressure ratio, ratio of specific heats, and temperature of jets differed.

Examination of shadowgraphs of sonic jet issuing from conical boat-tail bodies (ref. 11) indicated that the jet expands to the full base area or greater depending on jet pressure ratio. Jet static-pressure ratios for the present tests averaged approximately 3.65 which caused the jet to expand beyond the base area. Thus, with the jet issuing from the base, the external flow over the 7.5° boattail had to negotiate a flow deviation near the immediate vicinity of the base due to the expanded jet. When free-stream flow over the boattail is subsonic, positive pressure increments can be propagated upstream. It is believed that the external flow over the boattails for the power-on phases of the present tests was supersonic. To surmount this flow deviation imposed by the expanded jet, the flow over the rear portion of the boattail up to approximately $M = 1.2$ probably separates. This condition of flow separation will cause a shock wave to form in the external flow upstream of the base, giving rise to the occurrence of positive pressure increments on the boattail (see ref. 12). Another possible contributing factor to this reduction of drag at transonic and low supersonic speeds is the decrease in fin drag. When considering the location of the trailing

edge of the fins with respect to the bifurcated shocks (upstream limb and trailing wake), it is possible to have positive pressure increments acting on the trailing edge of the fins, hence also contributing toward reduction of drag.

Comparison of the average power-off total drag of the configurations with individual-model power-on drag is shown in figure 9. Although there does exist some deviation among the individual power-on drag-coefficient curves, the relative difference between them is considered to be generally small. It can be concluded from figure 9 that this range of jet sizes plays a minor role for this boattail angle and jet pressure ratio over most of the test Mach number range in reducing the drag.

Figure 10 contains plots of the change from power on to power off of base pressure coefficient ΔC_{p_b} and base drag coefficient ΔC_{D_b} as a function of area ratio of jet to base A_j/A_b for several Mach numbers. Figure 10(a) indicates that the jet effect on the base pressure coefficients becomes slightly more positive with increase in area ratio. Figure 10(b) shows that, although the change in base pressure coefficient increases slightly with area-ratio increase, the effect of increasing the annular area or decreasing the jet size appears to overshadow the pressure effect. Thus, the change in base drag coefficient decreases with increasing jet size. Also apparent for the models tested, $A_j/A_b = 0.563$ gave a maximum reduction in base drag coefficient from a power-on to a power-off condition.

An interesting comparison of the engine performance with sonic and computed supersonic exhaust nozzles can be made by using the data presented herein. A thrust coefficient was computed for a supersonic jet that expanded to free-stream static pressure and filled the entire base. It was assumed that the forebody drag was the same as that of the power-off condition. A net thrust coefficient of 1.159 was obtained at $M = 1.10$ by subtracting this power-off forebody drag from the computed thrust coefficient. The comparable flight test model with a sonic jet exhaust at the base had a net thrust coefficient of 1.189. Thus, it seems that in the transonic and low-supersonic speed range no apparent advantages would be gained by using a supersonic nozzle. Furthermore, from the standpoint of weight savings, it would be advantageous to use a sonic nozzle in this speed range.

CONCLUSIONS

In summarizing the results of the present tests, certain findings are of particular interest. The results obtained from the three similar flight models tested indicated the following:

1. In the transonic or low-supersonic speed range of this investigation, the jet affected the base and boattail pressures in such a manner as to cause an appreciable drag saving from the power-off condition.

2. In the higher supersonic speed range of the present tests, the jet influenced only the base pressures in such a manner as to cause drag reductions.

3. In the present tests, a change in jet diameter from 3.16 to 2.58 inches played a secondary role in the magnitude of power-on drag coefficient throughout the Mach number range studied.

Langley Aeronautical Laboratory,
    National Advisory Committee for Aeronautics,
        Langley Field, Va., May 19, 1955.

REFERENCES

1. De Moraes, Carlos A., and Nowitzky, Albin M.: Experimental Effects
      of Propulsive Jets and Afterbody Configurations on the Zero-Lift
      Drag of Bodies of Revolution at a Mach Number of 1.59. NACA
      RM L54C16, 1954.

2. Love, Eugene S.: Aerodynamic Investigation of a Parabolic Body of
      Revolution at Mach Number of 1.92 and Some Effects of an Annular
      Jet Exhausting From the Base. NACA RM L9K09, 1950.

3. Purser, Paul E., Thibodaux, Joseph G., and Jackson, H. Herbert:
      Note on Some Observed Effects of Rocket-Motor Operation on the
      Base Pressures of Bodies in Free Flight. NACA RM L50I18, 1950.

4. Cortright, Edgar M., Jr., and Kochendorfer, Fred D.: Jet Effects
      on Flow Over Afterbodies in Supersonic Stream. NACA RM E53H25,
      1953.

5. Gillespie, Warren, Jr.: Jet Effects on Pressures and Drags of
      Bodies. NACA RM L51J29, 1951.

6. Bressette, Walter E.: Investigation of the Jet Effects on a Flat
      Surface Downstream of the Exit of a Simulated Turbojet Nacelle
      at a Free-Stream Mach Number of 2.02. NACA RM L54E05a, 1954.

7. Cortright, Edgar M., Jr., and Schroeder, Albert H.: Investigation
      at Mach Number 1.91 of Side and Base Pressure Distributions Over
      Conical Boattails Without and With Jet Flow Issuing From Base.
      NACA RM E51F26, 1951.

8. Henry, Beverly Z., Jr., and Cahn, Maurice S.: Preliminary Results
      of an Investigation at Transonic Speeds To Determine the Effects
      of a Heated Propulsive Jet on the Drag Characteristics of a
      Related Series of Afterbodies. NACA RM L55A24a, 1955.

9. De Moraes, Carlos A., Hagginbothom, William K., Jr., and Falanga,
      Ralph A.: Design and Evaluation of a Turbojet Exhaust Simulator,
      Utilizing a Solid-Propellant Rocket Motor, for Use in Free-Flight
      Aerodynamic Research Models. NACA RM L54I15, 1954.

10. Wallskog, Harvey A., and Hart, Roger G.: Investigation of the Drag
      of Blunt-Nosed Bodies of Revolution in Free Flight at Mach Numbers
      From 0.6 to 2.3. NACA RM L53D14a, 1953.

11. Love, Eugene S., and Grigsby, Carl E.: Some Studies of Axisymmetric
    Free Jet Exhausting From Sonic and Supersonic Nozzles Into Still
    Air and Into Supersonic Streams. NACA RM L54L31, 1955.

12. Englert, Gerald W., Vargo, Donald J., and Cubbison, Robert W.:
    Effect of Jet-Nozzle-Expansion Ratio on Drag of Parabolic
    Afterbodies. NACA RM E54B12, 1954.
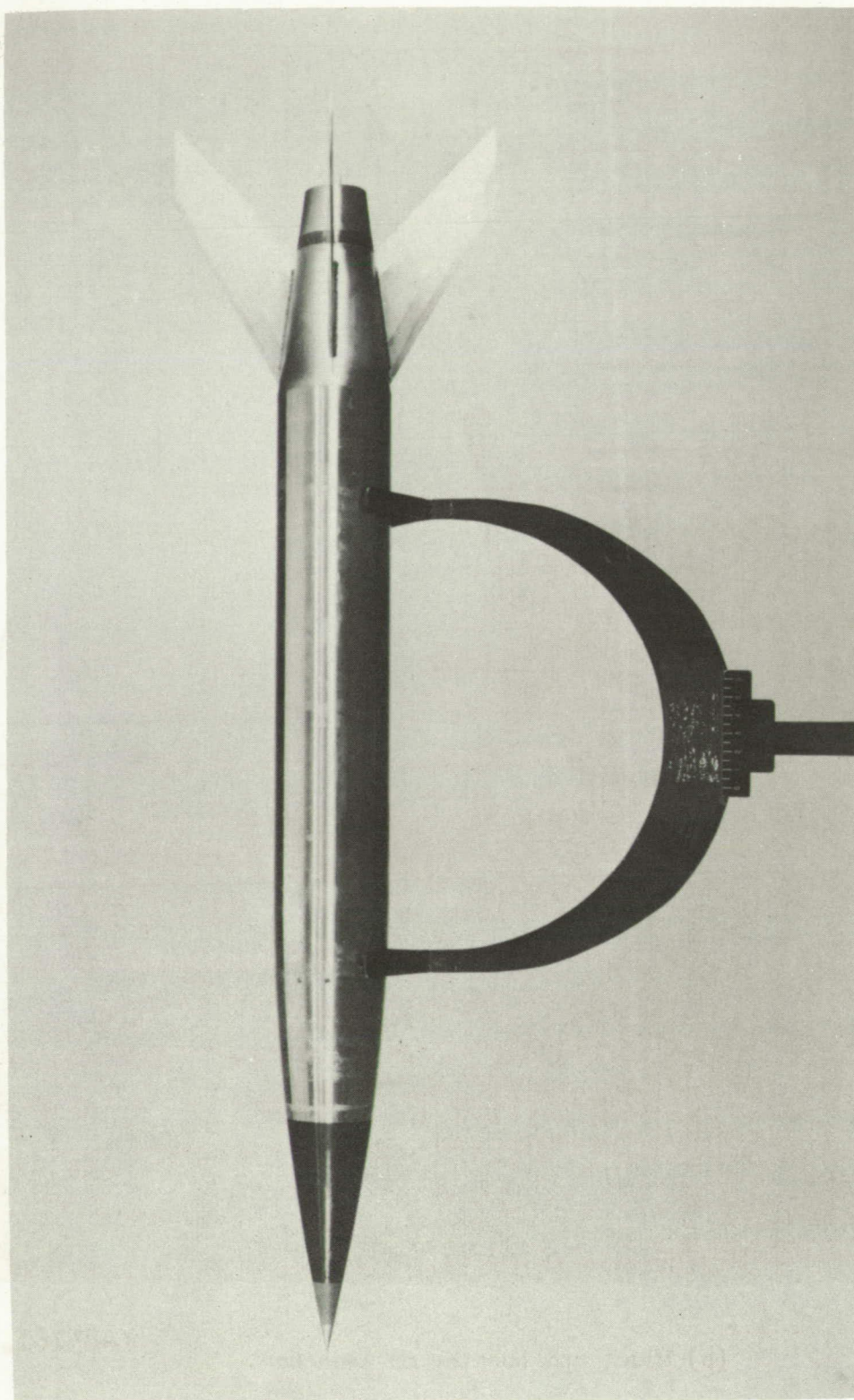
TABLE I.- COORDINATES OF PARABOLIC NOSE

[Station measured from fuselage nose]

Station, in.	Ordinate, in.
0	0
1	.245
2	.481
4	.923
6	1.327
10	2.019
14	2.558
18	2.942
22	3.173
26	3.250
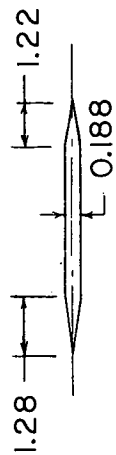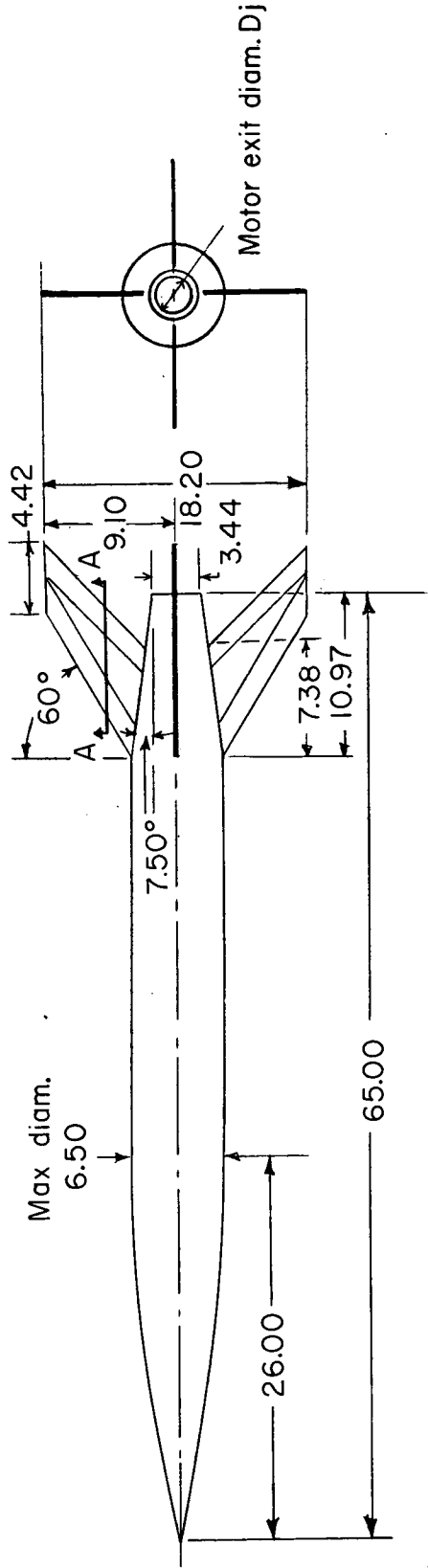
Model Number	Motor exit diam., Dj	A_j/A_b
1	3.160	.844
2	2.891	.706
3	2.582	.563

Figure 1.- External configuration of flight model. All dimensions are in inches.

L-82937.1

(a) Model alone.

Figure 2.- Photographs of flight models.
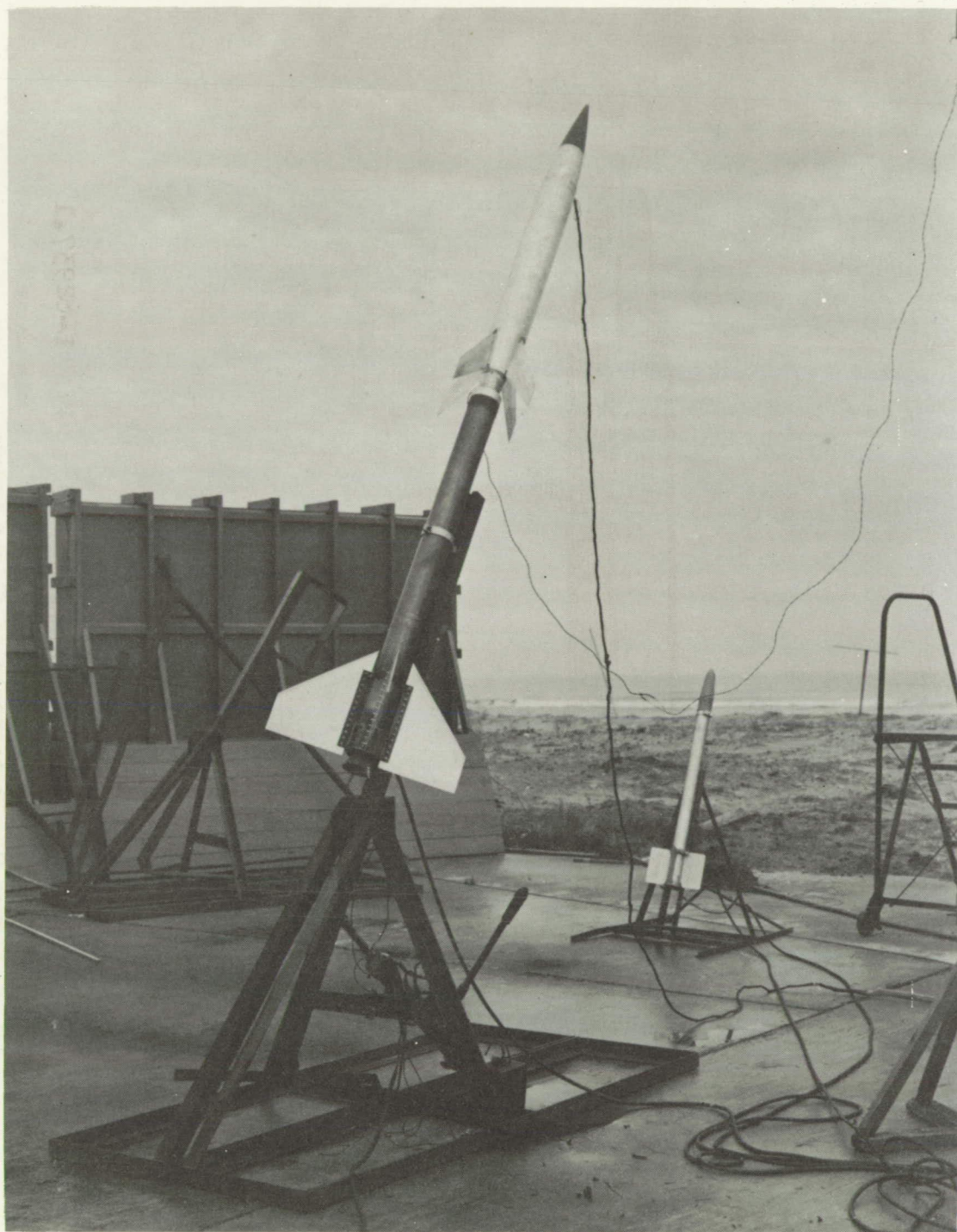
(b) Model and booster on launcher.

L-83161.1

Figure 2.- Concluded.
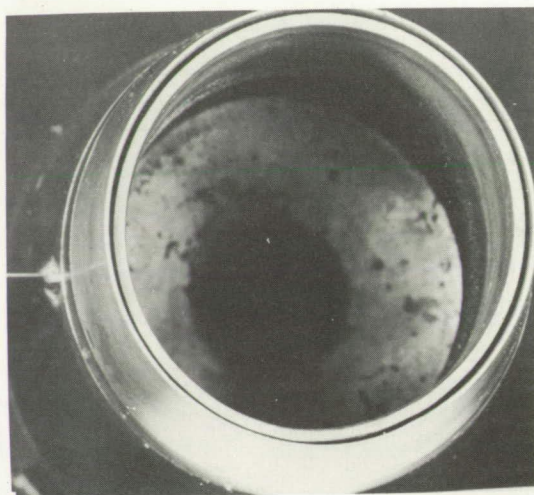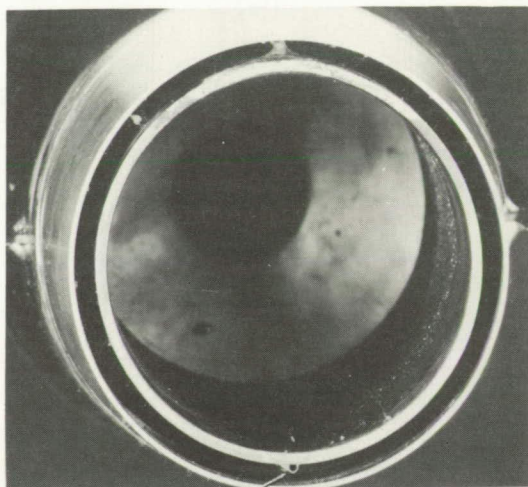
Model 1; $A_j/A_b = 0.844$ Base static-pressure tube   Model 2; $A_j/A_b = 0.706$
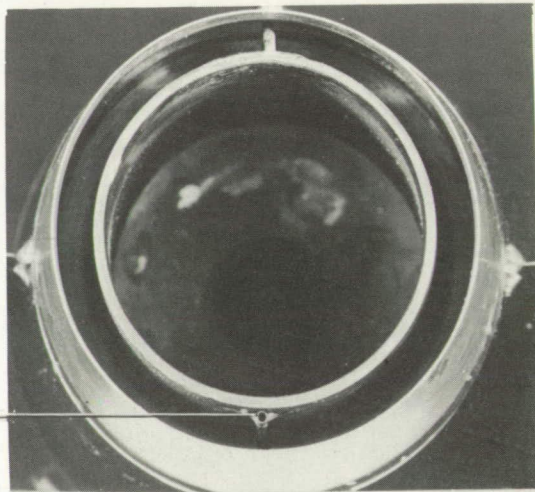
Base static-pressure tube

Model 3; $A_j/A_b = 0.563$

L-89307.1

Figure 3.- Photographs showing close-up views of the variation in base
annulus area for flight models tested.

Model Number	Throat Diameter	Exit Diameter
1	1.340"	3.160"
2	1.290"	2.891"
3	1.157"	2.582"
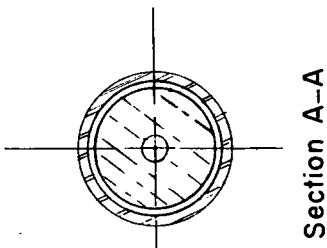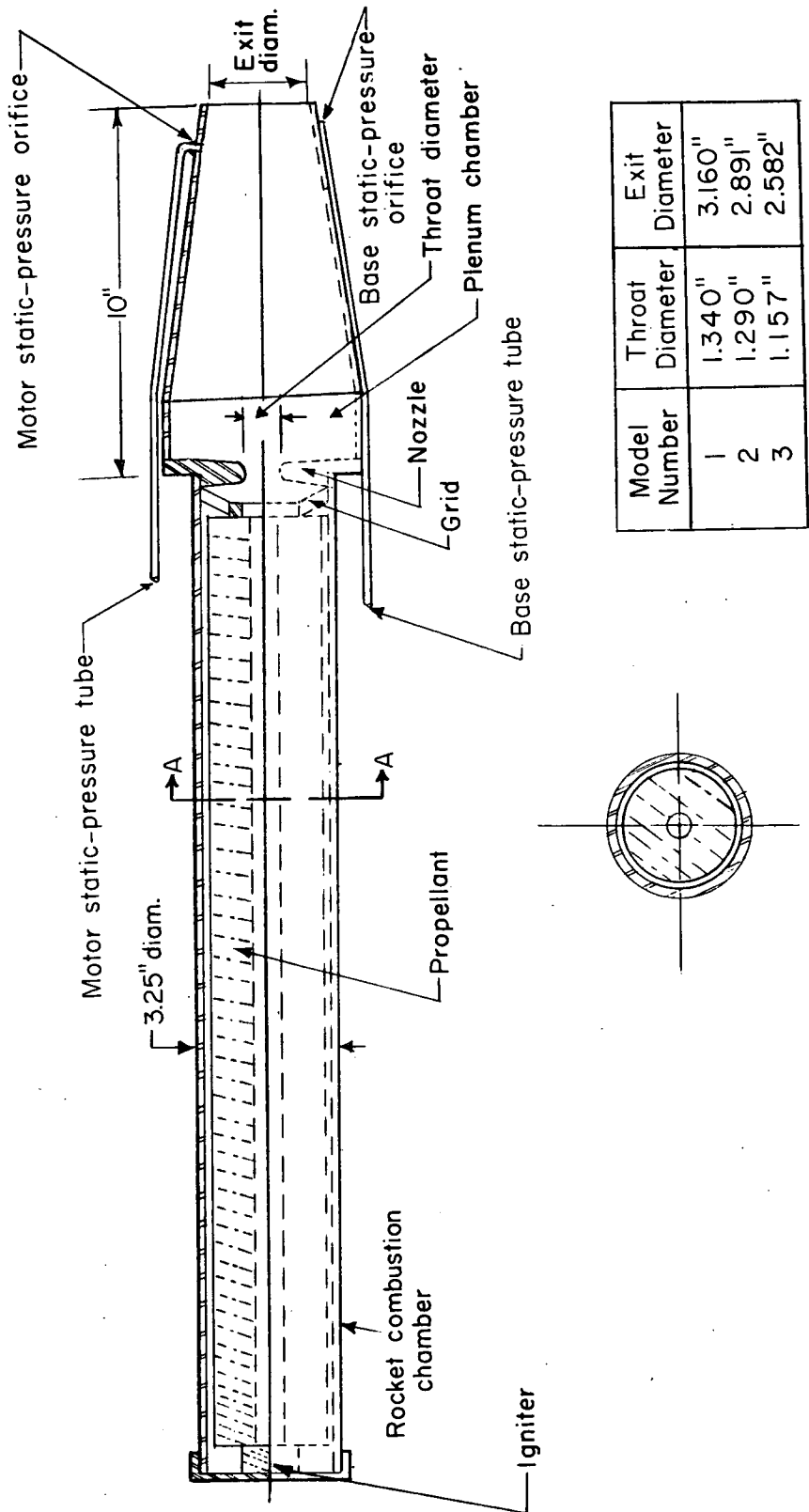
Figure 4.- Cross section of typical turbojet simulator.
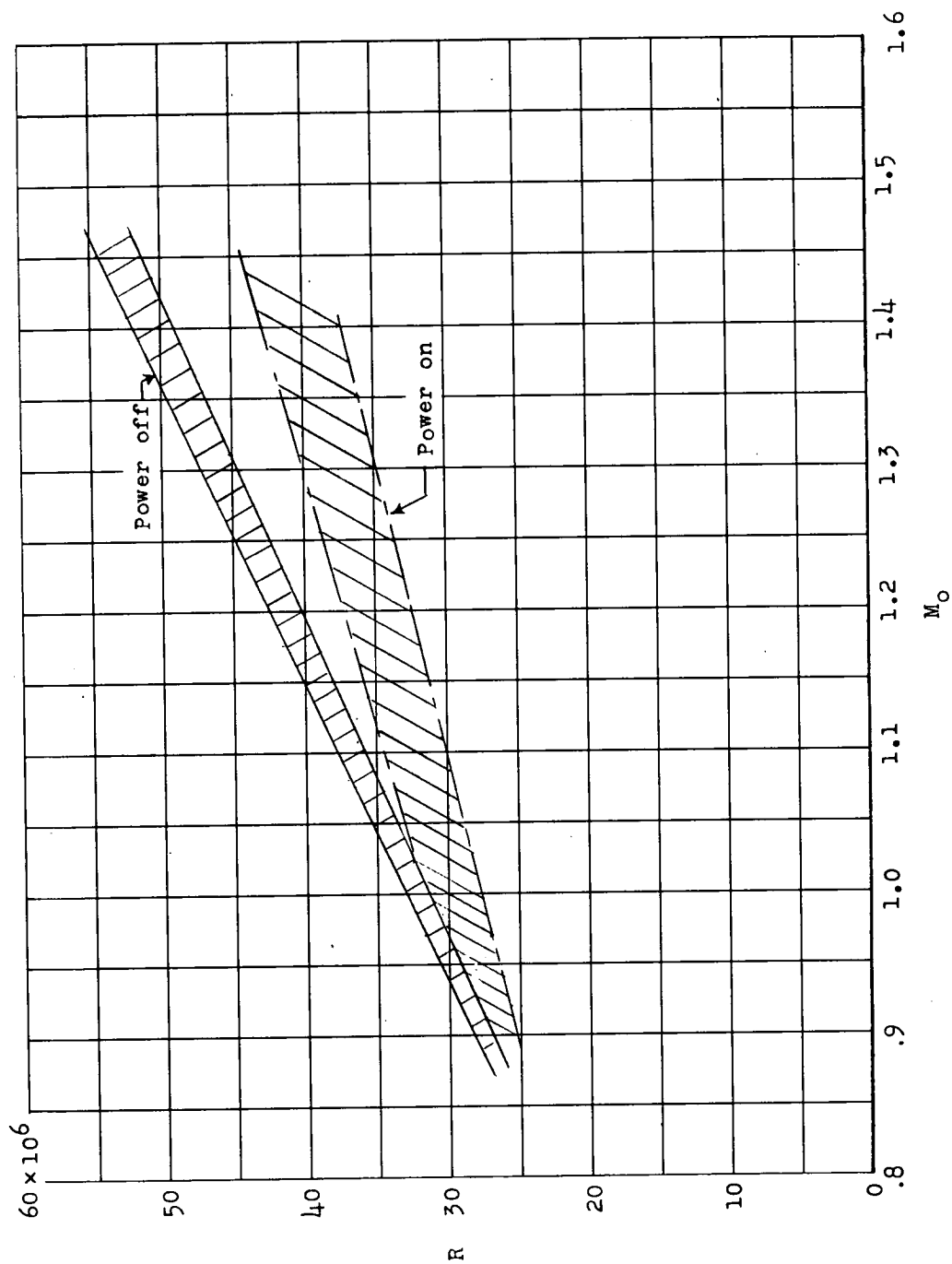
Figure 5.- Variation of Reynolds number with Mach number for models tested. Reynolds number is based on body length.
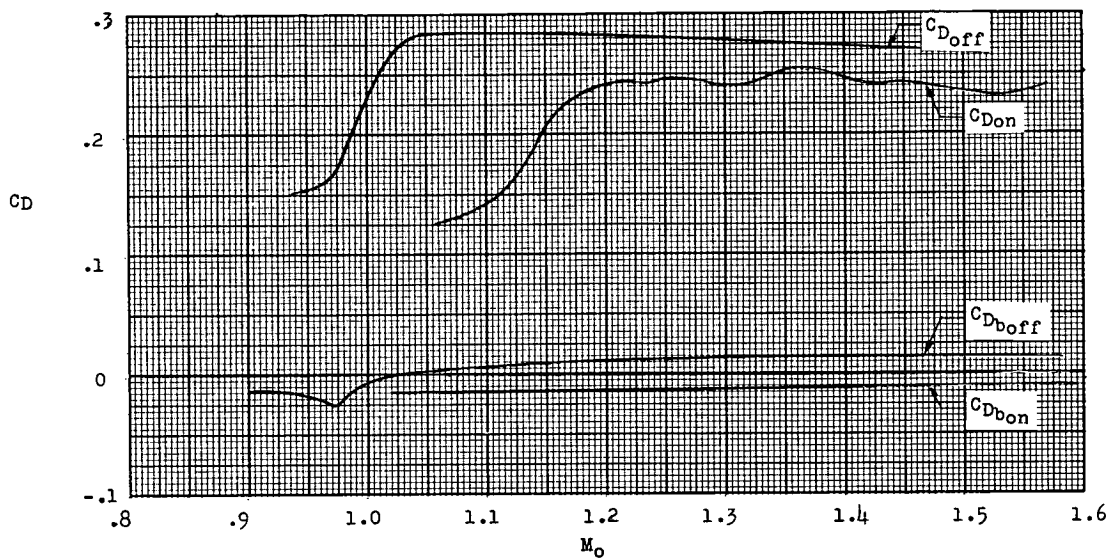
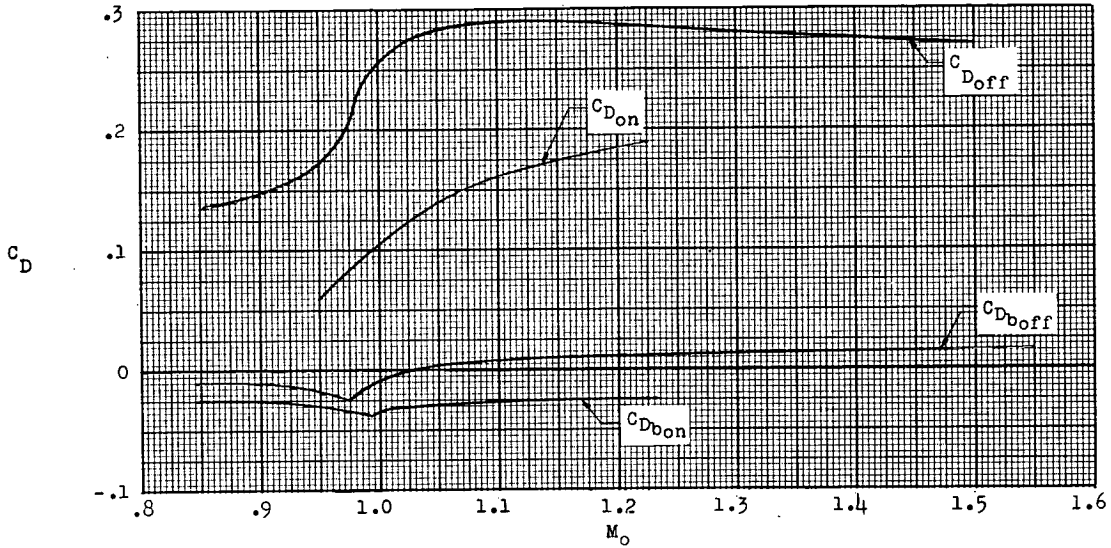(a) Total and base drag coefficients.
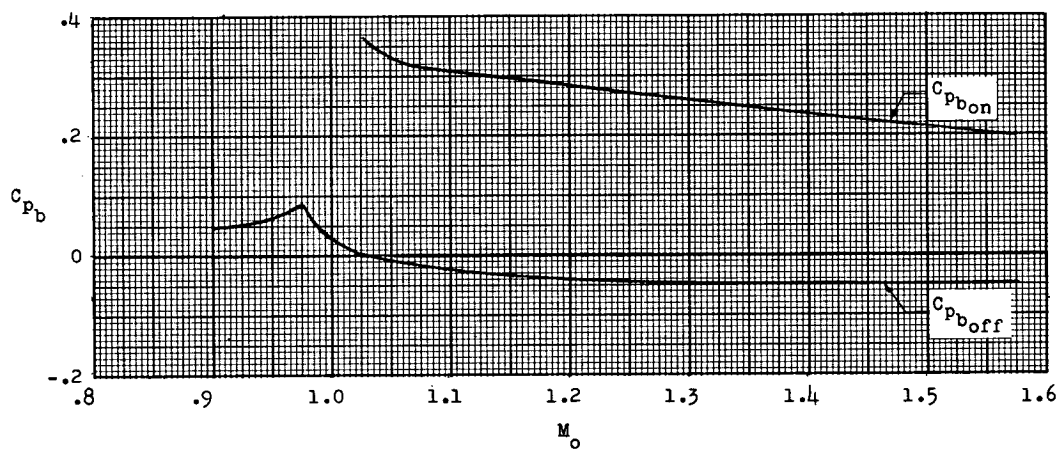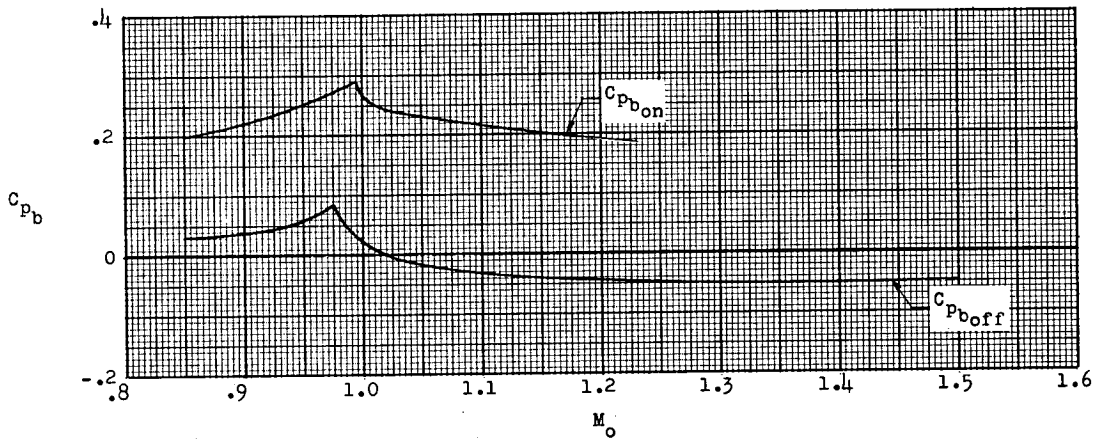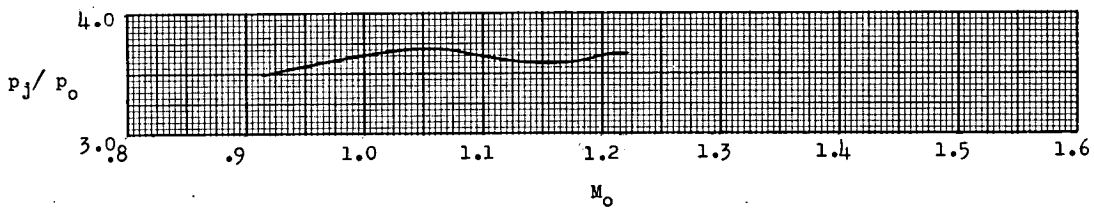
(b) Base pressure coefficient.
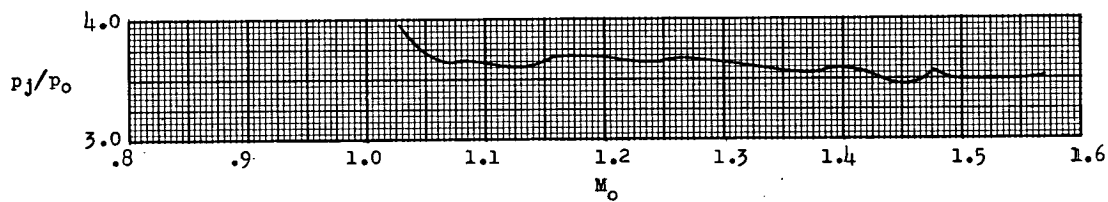
(c) Jet pressure ratio.

Figure 6.- Total and base drag coefficients, base pressure coefficient, and jet pressure ratio as a function of free-stream Mach number. Model 1 $\left(A_j/A_b = 0.844\right)$.
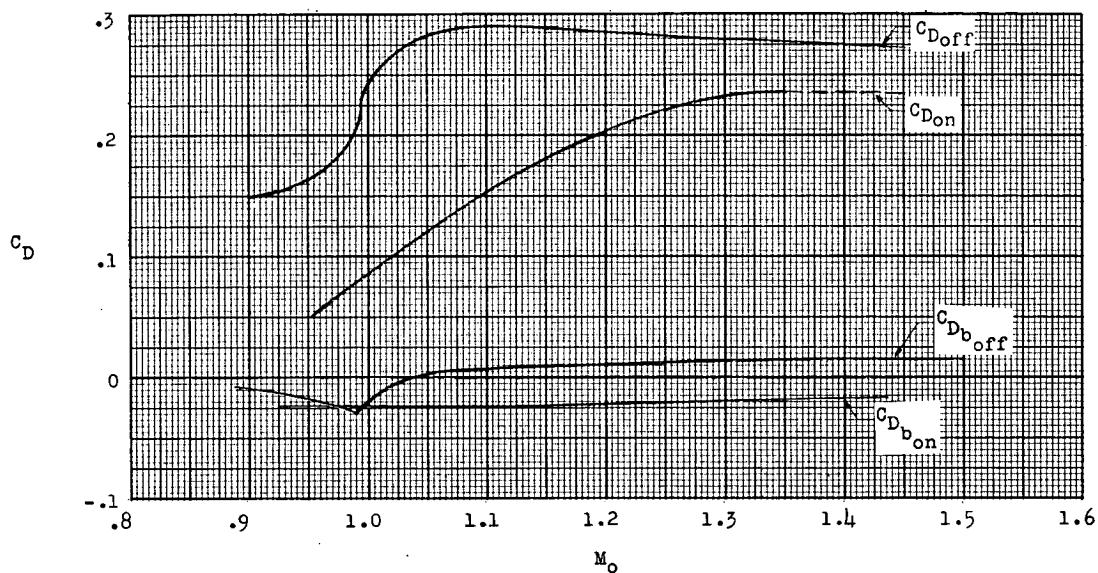
(a) Total and base drag coefficients.
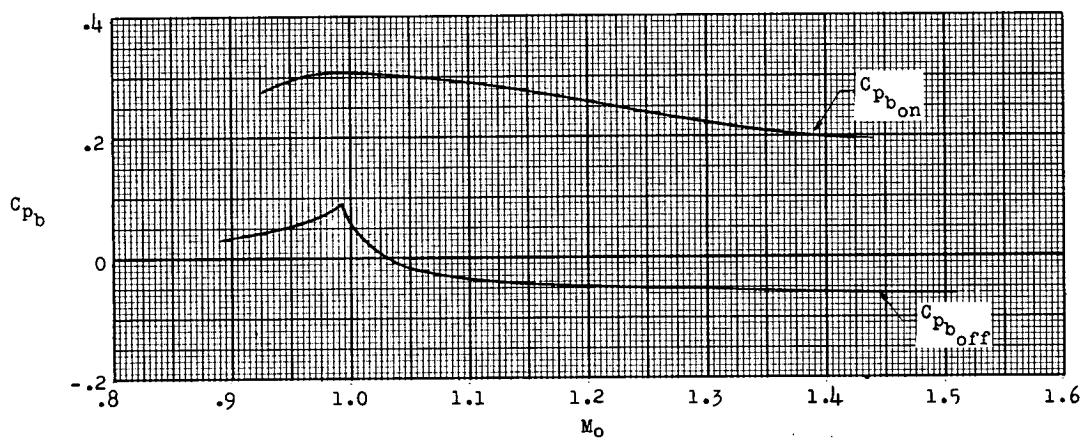
(b) Base pressure coefficient.
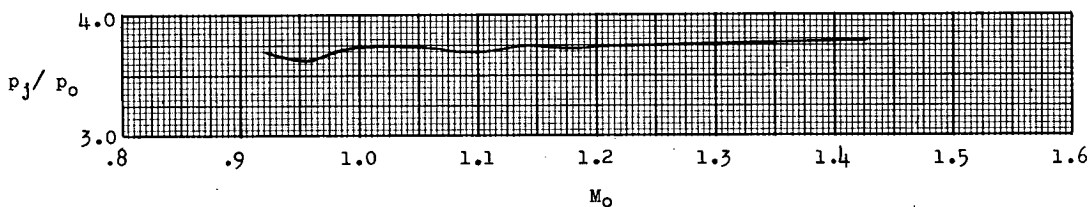
(c) Jet pressure ratio.

Figure 7.- Total and base drag coefficients, base pressure coefficient, and jet pressure ratio as a function of free-stream Mach number. Model 2 $\left(A_j/A_b = 0.706\right)$.

(a) Total and base drag coefficient.

(b) Base pressure coefficient.

(c) Jet pressure ratio.

Figure 8.- Total and base drag coefficients, base pressure coefficient, and jet pressure ratio as a function of free-stream Mach number. Model 3 $\left(A_j/A_b = 0.563\right)$.
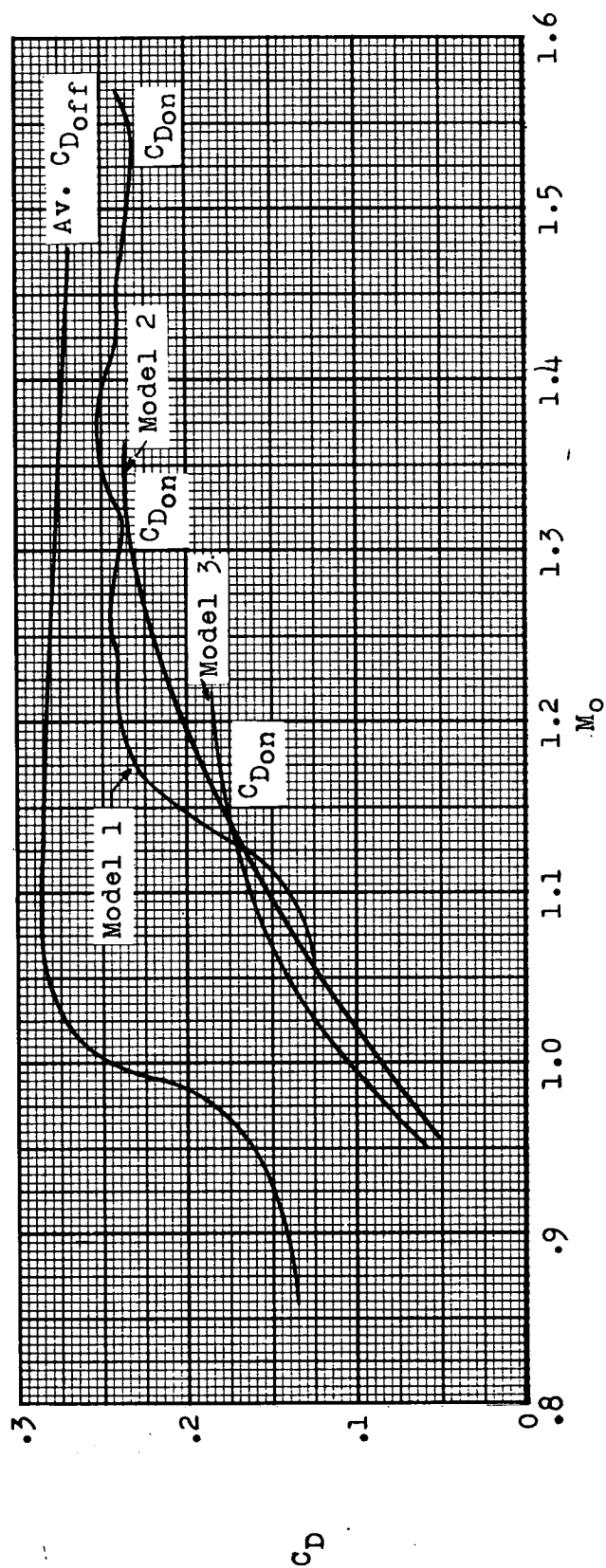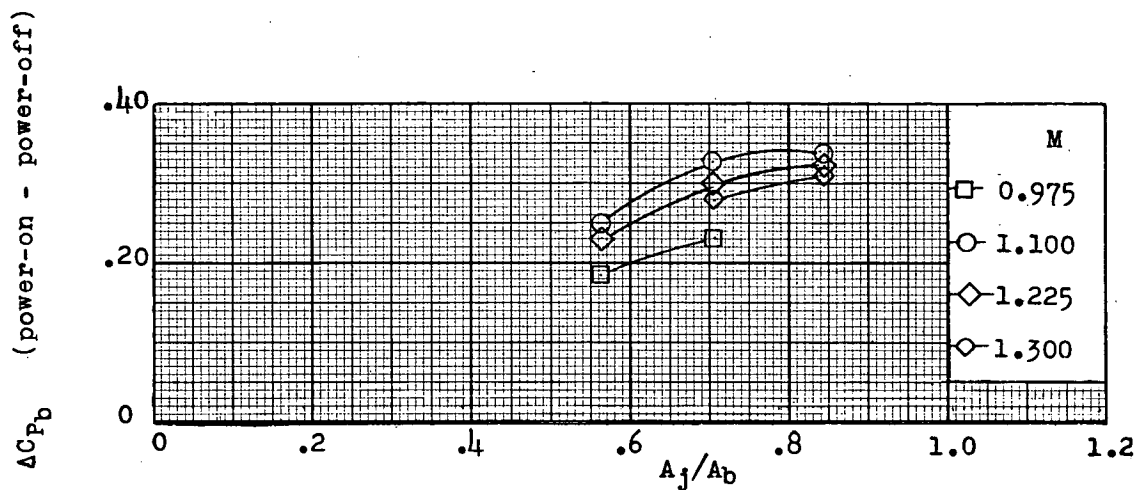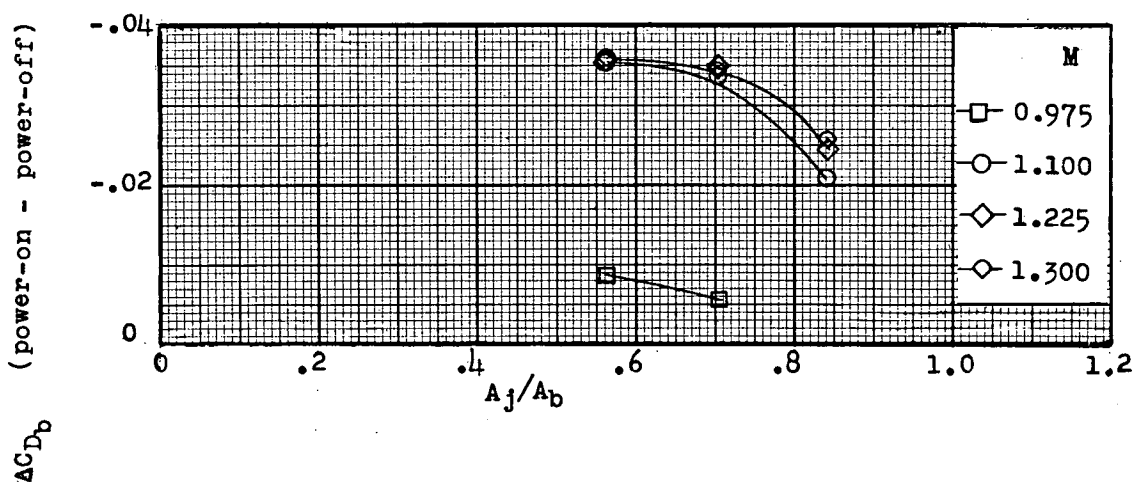
Figure 9.- Comparison of power-off and power-on drag coefficients.

ΔCP_b (power-on - power-off)

M
□ 0.975
○ 1.100
◇ 1.225
◇ 1.300

A_j/A_b

(a) Variation of the change in base pressure coefficient as a function of area ratio of jet to base.

ΔCD_b (power-on - power-off)

M
□ 0.975
○ 1.100
◇ 1.225
◇ 1.300

A_j/A_b

(b) Variation of the change in base drag coefficient as a function of area ratio of jet to base.

Figure 10.- Variation of the change in base pressure coefficient and base drag coefficient for various Mach numbers as a function of area ratio of jet to base.